Two-stub quarter wave superconducting resonator design

N. R. Lobanov and D. C. Weisser

Department of Nuclear Physics, Research School of Physical Sciences and Engineering, Australian National University, Canberra, ACT 0200, Australia

(Received 5 March 2006; published 24 April 2006)

This paper describes the electromagnetic and mechanical properties of a 150 MHz $\lambda/4$, 3-gap structure with two loading elements, for the velocity range $\beta = 0.04$–0.12 in the context of TEM-like $\lambda/4$ and $\lambda/2$ structures with multiple loading elements. A simple transmission lines model is presented and the results of Micro Wave Studio and simulations are discussed. The column of the multistub structures opens the opportunity to minimize current in locations allowing the exploitation of demountable joints and control the frequency splitting between the accelerating and other modes. These resonators are appropriate for the upgrade of the medium- and high-velocity sections of the ANU Heavy-Ion Accelerator Facility. Because of the broad velocity range for which such structures can be tailored, they can also be used in spallation neutron sources and rare isotope accelerators.

DOI: 10.1103/PhysRevSTAB.9.042002 PACS numbers: 29.17.+w, 29.27.−a, 41.75.−i

I. INTRODUCTION

The growing interest in medium energy heavy-ion and proton accelerators has spawned a sustained worldwide effort dedicated to the development of appropriate superconducting accelerating structures. The majority of the structures in use or under development fall into two broad categories: those based on a Transverse Electric and Magnetic mode (TEM-like) and those based on a Transverse Magnetic mode (TM-like). TEM-like resonators can be separated into those characterized by quarter-wavelength transmission lines (QWR, $\lambda/4$) and by half-wavelength (HWR, $\lambda/2$) transmission lines.

The $\lambda/4$ structures include single straight loading elements, as in the original quarter-wave resonator 1-QWR [1] or a spiral element [2]. There are two straight elements in the twin quarter-wave resonator 2-QWR [3] and curved ones in the split-ring resonator [4]. One element may be rotated by an arbitrary angle α to the next one as in spoke cavities [5–7], where the loading elements are 90° from one another. When the number of loading elements is large, the cavity is referred to as a CH-, H-, or IH-type cavity [8].

If the number of the loading elements is two or more, they can be mounted on a supporting column as in the split ring [4] and in the two- and three-stub resonators [9,10]. In these designs, the frequency of the nonaccelerating mode is shifted substantially lower than the accelerating mode frequency. In the design of the 2-QWR described here, the H field at the edge of the shorting plate is reduced to a few percent of the peak magnetic field, H_p, by choosing the appropriate length for the supporting column.

In the ladder cavity, with straight loading elements and $\alpha = 0$, the H field in the outer conductor area parallel to the plane of loading arms, can also be reduced to a few percent of H_p [11]. The low magnetic field, and so low current, opens the possibility of employing demountable flanges, since the low current will not degrade excessively the performance of the resonator. Demountable flanges allow access for manufacture, surface treatment, and repairs.

As the number of loading elements n increases, the velocity acceptance range of the resonator decreases proportionally to $1/n$. Although in this paper both $\lambda/4$ and $\lambda/2$ structures with $n = 2$ are considered, the same design concepts could be applied to cavities with more than 2 loading elements.

The drift tubes, through which the beam passes, are mounted on the loading elements and can be quite elaborate. Two examples are the radio frequency quadruple vanes as in the ATLAS RFQ split ring [12] and the bifurcated drift tubes as in the ATLAS interdigital quarter-wave cavities [13].

Some existing and possible $\lambda/4$ and $\lambda/2$ cavities with straight loading elements are listed in Table I.

In Table I, the entries in italics are structures not yet investigated. Subscript "c" stands for design of loading elements incorporating a supporting column. Note that there are also $\lambda/4$ and $\lambda/2$ cavities based on arbitrary angle $\alpha \neq 0$ which are not listed here.

Cavities with low stored energy are tuned capacitively by deflection of the tuning plates opposite the free ends of the loading arms. As will be discussed elsewhere, cavities

TABLE I. Possible $\lambda/4$ and $\lambda/2$ cavities.

$\lambda/4$	$\alpha = 0°$	1-QWR [1]	2-QWR [3]	3-QWR
		⋯	2-QWR$_c$ [9]	3-QWR$_c$ [10]
	$\alpha = 90°$	⋯	2-QWR$_\alpha$	3-QWR$_\alpha$
$\lambda/2$	$\alpha = 0°$	1-HWR [5]	*2-HWR*	3-HWR [11]
		⋯	2-HWR$_c$	3-HWR$_c$
	$\alpha = 90°$	1-spoke [5]	2-spoke [6]	3-spoke [7]

with two loading elements can be tuned with a rotary tuner of a new design.

II. TWO-STUB RESONATOR

This report introduces the twin $\lambda/4$ resonator concept incorporating a supporting column to control eigenfrequency splitting and to minimize current in the joint to a demountable flange. The demountable flange facilitates fabrication so that electron beam welding and vacuum brazing are not required. The design of a 150 MHz, $\lambda/4$, 4-gap structure with three loading elements will be presented elsewhere.

A. Transmission line approximation

The gap lengths, g in the two-stub resonator, 2-QWR, are in the ratio 1:2:1 as seen in Fig. 1 and therefore the E fields are all equal, with $E = E_1 = V_0/g = E_2 = 2V_0/2g = E_3 = V_0/g$, where V_0 is the voltage generated by the loading elements. The accelerating field is $E_{\rm acc} = \Delta E/qL$, where ΔE is the energy gain and q is the charge state. $L = l + 2r_a$ is the beam path length, where l is the cavity physical length along beam axis and r_a is the radius of beam aperture. We have chosen to study a three gap structure that produces $E_{\rm acc} = 4.7$ MV/m for $L = 0.17$ m and $V_0 = 0.2$ MV.

We can approximate the equivalent coaxial transmission line for each stub separately of the 2-QWR cavity since the symmetry plane between the stubs is an equipotential equivalent to a ground plane. The outer conductor's effective diameter can be taken to be the average of the diameter, $D = 16$ cm, and the distance from the symmetry plane to the wall, $D/2$, i.e., $D_{\rm eff} = 12$ cm. The inner conductor corresponds to an effective diameter $d_{\rm eff} = (a + b)/2 = 4$ cm. The characteristic impedance of a coaxial transmission line (CTL) is $Z_0 = 60 \times \ln[D_{\rm eff}/d_{\rm eff}] = 66\Omega$. The maximum current at the shorted end $I_0 = V_0/Z_0 = 3030A$ at $E_{\rm acc} = 4.7$ MV/m. The physical length l of a C_l-loaded quarter-wave CTL is $l = 0.16\lambda \times \tan^{-1}(5.3 \times 10^{-8}\lambda/C_l Z_0) = 40.4$ cm at $C_l = 5$ pF, where λ is the rf wavelength.

B. Optimization design with Microwave Studio (MWS)

The 2-QWR has two principal low frequency rf eigenmodes. The first one is a nonaccelerating mode, mode 1, in which surface charge oscillates from the drift tubes in parallel and then to the outer cylinder, as shown in Fig. 2. Mode 1 is analogous to a QWR with a high H field in the shorting plate. The second mode is the accelerating mode, mode 2, in which surface charge oscillates along the stubs from one beam drift tube to the other, as illustrated in Fig. 3.

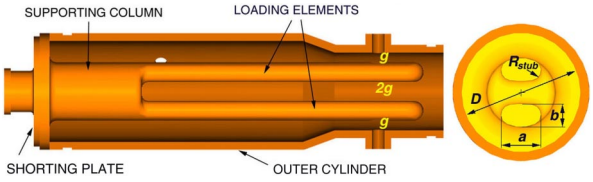

FIG. 1. (Color) A 150 MHz 2-QWR cavity, with $\beta = 0.06$.

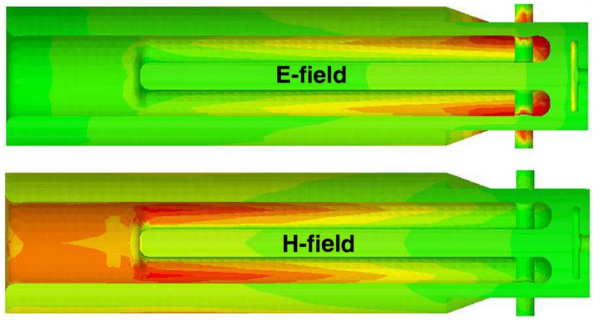

FIG. 2. (Color) Nonaccelerating mode 1 for E field and H field in a 2-QWR. Red represents high values of fields of the same polarity.

The peak electric surface field E_p occurs at the end of each stub and depends on the end curvature and stub edge-radius $R_{\rm stub}$. The MWS-calculated relative accelerating field profile E_z along beam axis is shown in Fig. 4, with $E_{\rm acc}$ obtained by integrating E_z resulting in $E_p/E_{\rm acc} = 5.4$. For $\lambda/2$ structures, the peak surface electric field occurs at the center of the loading element and a typical $E_p/E_{\rm acc}$ ratio of 3.3 independent of β can be obtained [14]. For $\lambda/4$ structures, the ratio of 4.5 to 5.0 is reported in the review paper of Ref. [14].

The only available parameter to minimize H_p is $R_{\rm stub}$, shown in Fig. 1. Increasing this radius not only opens more space for the H field, but also importantly, makes more uniform the distribution of the current around the circumference. A value for $H_p/E_{\rm acc}$ of 13.6 mT/MV/m was calculated with the MWS simulation code for $R_{\rm stub} = 12$ mm. No substantial improvement of $H_p/E_{\rm acc}$ was ob-

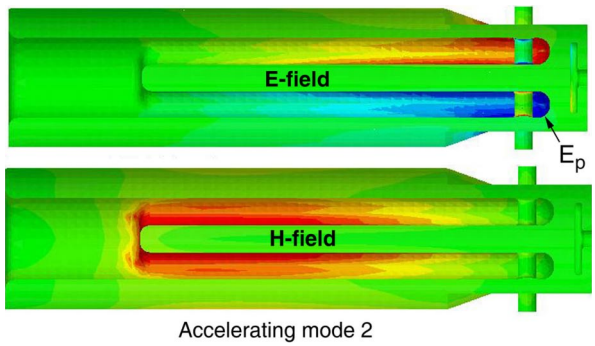

FIG. 3. (Color) Accelerating mode 2 for E field and H field in a 2-QWR. Blue represents the opposite polarity to red.

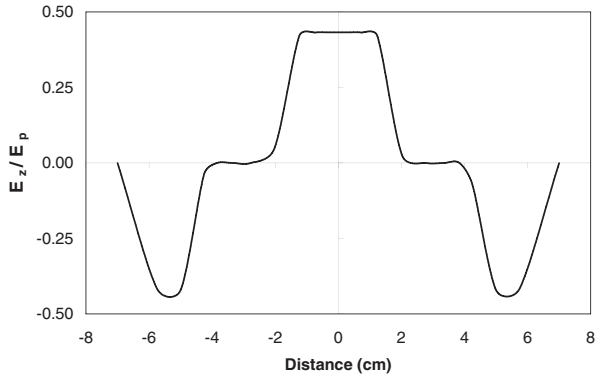

FIG. 4. The ratio of the accelerating field E_z to the peak field E_p obtained with MWS, as a function of the distance along the beam axis z in a 2-QWR.

tained by introduction of a 3 to 5 mm fillet radius at the interface between the stubs and supporting column or by tapering the stub width from 52 mm at the top to 70 mm at the bottom.

The distribution of the magnetic field for mode 2 can be used to locate the highest field region, which sets a limit to the maximum accelerating capability of a resonator for a given superconducting material.

For $\lambda/2$ structures, the maximum magnetic field occurs where the loading element meets the outer enclosure. As in case of the electric field, substantial deviations from the 7 to 8 mT at 1 MV/m calculated by MWS have been reported. For low-velocity $\lambda/4$ structures, a typical value up to 13 mT at 1 MV/m is reported in the review paper of Ref. [14]. The results of MWS numerical simulations of 2-QWR are summarized in Table II.

Setting the maximum peak fields at 4.2 K for lead film at $E_p = 20$ MV/m and $B_p = 53$ mT, then the peak electric field limits the accelerating field to $E_{\mathrm{acc}} = 20/5.4 = 3.7$ MV/m. Similarly, the acceleration field due to the B_p limit is $E_{\mathrm{acc}} = 53/13.6 = 3.9$ MV/m. Therefore the performance of a lead plated 2-QWR is expected to be limited by the E_p at $E_{\mathrm{acc}} = 3.7$ MV/m.

In contrast, for solid Nb the reported surface electric field at 4.2 K is $E_p = 60$ MV/m and the peak magnetic field is $B_p = 120$ mT. This implies the upper values to the accelerating field of $E_{\mathrm{acc}} = 60/5.4 = 11.1$ MV/m for the E_p limit and $E_{\mathrm{acc}} = 120/13.6 = 8.8$ MV/m for the B_p limit. Thus the Nb 2-QWR resonator performance is expected to be limited by the B_p at $E_{\mathrm{acc}} = 8.8$ MV/m.

These limits for both lead and niobium should be considered indicative since the MWS calculation for E_p/E_{acc} and B_p/E_{acc} may be underestimated and the maximum assumed peak fields may be overstated.

TABLE II. 2-QWR, rf parameters.

Mode 2 frequency at 300 K	152.071 MHz
Mode 1 frequency at 300 K	119.455 MHz
β_{opt}	0.06
E_p/E_{acc}	5.4
B_p/E_{acc}	13.6 mT/(MV/m)
Stored energy, at $E_{\mathrm{acc}} = 1$ MV/m	28.4 mJ/(MV/m)^2
E_{acc} at $J = 1$ J	5.9 MV/m
$\Gamma = \mathrm{QR}_s$	18 Ω

C. Structural properties

During the resonator operation, variations in the electric field amplitude and phase due to microphonics are addressed by the rf control system. To minimize the power needed for the control systems the resonator should be as stiff as possible. Stiff structures have high mechanical vibration frequencies. Since environmental mechanical noise is usually low frequency, it is desirable to have the lowest structural resonance frequencies well above the environmental frequencies. Finite element structural analyses (STRAND7) [15] identified the four lowest mechanical modes, shown in Fig. 5.

The first two are bending modes of the stubs in which the drift tubes move in the same direction (mode 1, 77 Hz) and opposite (mode 2, 80 Hz) direction along the beam line. The second two are traverse-bending modes of the stubs where the drift tubes move together (mode 3, 120 Hz) and opposite (mode 4, 135 Hz) in planes perpendicular to the beam axis. Since the stubs themselves and the supporting column are quite stiff, the frequencies of modes 1 and 3 are strongly affected by distortion of the shorting plate on which the column is mounted. The lowest axial mode was raised from 72 to 77 Hz and the lowest traverse mode from 105 to 120 Hz by increasing the shorting plate thickness from 10 to 25 mm.

D. Demountable flange joints

The 2-QWR employs two demountable flange joints. One is between the shorting plate and the outer conductor and the other is between the tuner plate and the outer conductor. For a 137 mm long supporting column, the MWS-calculated H field, H_{joint}/H_p, in the shorting plate

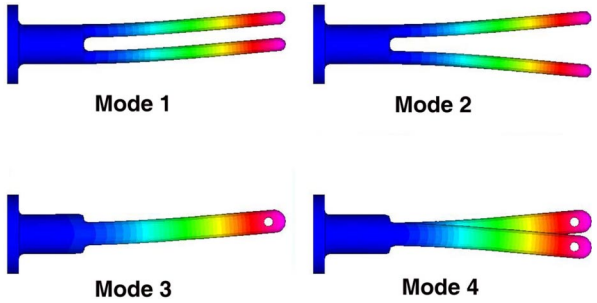

FIG. 5. (Color) The four lowest mechanical modes in the 2-QWR.

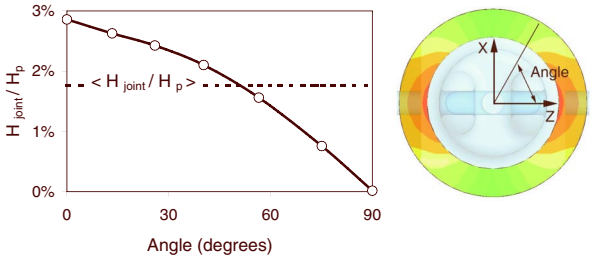

FIG. 6. (Color) The MWS-calculated distribution of mode 2, H field H_{joint}/H_p in the 2-QWR rf shorting plate joint. The average value of ratio $\langle H_{\text{joint}}/H_p \rangle$ is 1.76%.

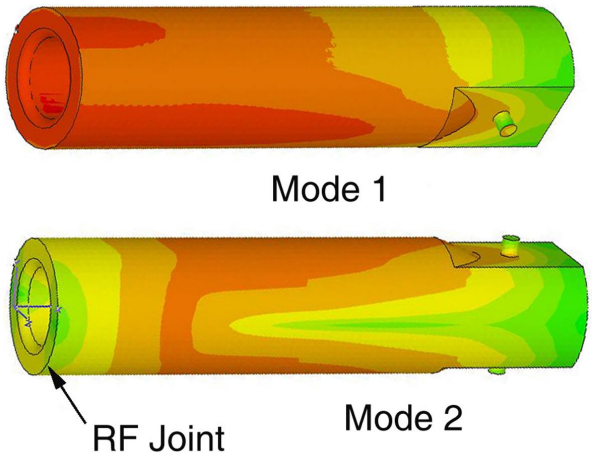

FIG. 7. (Color) Calculated low frequency accelerating mode 2 for H field in 2-QRWs outer can.

joint for mode 2 is shown in Fig. 6. The rf joint is in a region of low current density at the edge of the shorting plate. This ratio $(H_{\text{joint}}/H_p)_{\text{max}}$ does not exceed 3% and $H_{\text{joint}} < 1.8$ mT at $H_p = 64$ mT at 4.7 MV/m.

The MWS distribution of H field in the outer conductor for both mode 1 and mode 2 is shown in Fig. 7. For mode 2, as the supporting column is lengthened, the currents going in the opposite direction in the outer conductor walls flow more in the wall, and less current returns to the stub assembly through the joint. It is this feature of the two-stub resonator design that allows the minimization of rf current through the shorting plate joint. The length of the support column of the rotary tuner has a similar effect on the current in the tuner plate joint [15].

The 2-QWR design minimizes H field in the rf gaskets in mode 2, which is in marked contrast to the high rf current at the shorting plate to outer conductor for mode 1.

III. CONCLUSION

The MWS calculations for the 2-QWR indicate relatively low peak surface electric field ratio of $E_p/E_{\text{acc}} = 5.4$ MV/MV/m as compared to conventional resonators. The peak magnetic field ratio is also low at $H_p/E_{\text{acc}} = 13.6$ mT/MV/m.

The frequencies of the lowest mechanical modes are strongly affected by the distortion of the shorting plate and are above 77 Hz for a 25 mm thick plate. High stiffness combined with low energy content provides mechanical stability against microphonics. Thus rf stabilization of a self-excited loop by addition of a signal in quadrature is adequate.

The use of a column between the stubs and the shorting plate in multistub cavities provides a tool to achieve low H fields, below 2 mT at 4.7 MV/m, where the outer conductor joins the shorting plate. This enables the use of a removable flange connected, with an rf gasket, which allows easy access to the interior of the resonator for manufacture, inspection, mechanical polishing, chemical surface treatment, high pressure rinsing, coating, and repair. The free choice of the column length enables the frequency of nonaccelerating mode to be shifted 33 MHz below the accelerating mode frequency.

The multistub resonators also intrinsically have low currents between the outer conductor and the tuner flange. This allows the use of a rotary tuner of new design instead of the conventional deflection plate. The small driving force required for a rotary tuner, compared to the force needed to deflect a conventional plate, can be provided with a low-backlash mechanism.

Exploitation of a suite of such resonators would extend the mass and energy ranges for the heavy-ion facility at the ANU. It can be also used for the very low energy section of a high current proton Linac [16] or heavy-ion accelerators [17].

ACKNOWLEDGMENTS

The competence and skills of Alistair Muirhead in the use of Mechanical Desktop has been a key issue for the advancement of the project. We thank Jouris Fourier and Benoit Gay for their contribution in simulating mechanical properties of the resonator. The authors thank Computer-Simulation Technology GmbH for providing an evaluation license for package MWS to Nuclear Physics Department and Dr. Frank Demming-Janssen, CST Headquarters, for his generous advise, cooperation, and enthusiasm during this work.

[1] D. W. Storm, J. M. Brennan, and I. Ben-Zvi, IEEE Trans. Nucl. Sci. **32**, 3607 (1985).
[2] G. I. Dick and K. W. Shepard, in Proceedings of the Applied Superconductivity Conference, Annapolis, MD, 1972, Institute of Electrical and Electronics Engineers Pub. No. 72CHO682, p. 649.
[3] J. R. Delayen and J. E. Mercereau, Nucl. Instrum. Methods Phys. Res., Sect. A **257**, 71 (1987).
[4] K. W. Shepard, J. E. Mercereau, and G. J. Dick, IEEE Trans. Nucl. Sci. **22**, 1179 (1975).

[5] J. R. Delayen, in Proceedings of the 1988 Linear Accelerator Conference, Virginia, Continuous Electron Beam Accelerator Facility Report No. CEBAF-Report-89-001, 1989, p. 199.

[6] J. R. Delayen, C. L. Bohn, and C. T. Roche, in *Proceedings of the LINAC'90 Conference, Albuquerque, NM, 1990* (Los Alamos National Laboratory, Albuquerque, NM, 1991), p. 82.

[7] K. W. Shepard and P. N. Ostroumov, Phys. Rev. ST Accel. Beams **6**, 080101 (2003).

[8] R. Eichhorn and U. Ratzinger, in *Proceedings of the 10th Workshop on RF Superconductivity, KEK, Japan, 2001*, edited by S. Noguchi (KEK, Tsukuba, Japan, 2003), p. 20.

[9] N. R. Lobanov and D. C. Weisser, in *Proceedings of the 32nd Symposium of North Eastern Accelerator Personnel, 1999*, edited by D. K. Hensley (Oak Ridge National Laboratory, Oak Ridge, TN, 1999), p. 255.

[10] N. R. Lobanov and D. C. Weisser, in *Proceedings of the 9th Workshop on RF Superconductivity, Santa Fe, NM, 1999*, edited by B. Rusnak (LANL, Los Alamos, NM, 2000), p. 124.

[11] A. Pisent, G. Bisoffi, M. Comunian, A. Facco, and E. Fagotti, in *Proceedings of the 8th European Particle Accelerator Conference, Paris, 2002* (EPS-IGA and CERN, Geneva, 2002), p. 939.

[12] J. R. Delayen and K. W. Shepard, Appl. Phys. Lett. **57**, 514 (1990).

[13] K. W. Shepard, in *Proceedings of the 1986 Linac Conference, Stanford, CA* (Stanford Linear Accelerator Center, SLAC-303, Stanford, CA, 1986), p. 269; http://www.slac.stanford.edu/pubs/slacreports/slac-r-303.html

[14] J. R. Delayen, in *Proceedings of the 10th Workshop on RF Superconductivity, KEK, Japan, 2001* (Ref. [8]), p. 152.

[15] N. R. Lobanov and D. C. Weisser, in Proceedings of the Australian Institute of Physics, 16th Biennial Congress, Australian National University, Canberra, Australia, 2005.

[16] G. W. Foster, in Proceedings of the 12th Workshop on RF Superconductivity, Ithaca, NY, 2005 (to be published).

[17] M. P. Kelly, in Ref. [16].